

## Lipid Models for United-Atom Molecular Dynamics Simulations of Proteins

Andreas Kukol\*

*School of Life Sciences, University of Hertfordshire, Hatfield AL10 9AB, United Kingdom*

Received August 21, 2008

**Abstract:** United-atom force fields for molecular dynamics (MD) simulations provide a higher computational efficiency, especially in lipid membrane simulations, with little sacrifice in accuracy, when compared to all-atom force fields. Excellent united-atom lipid models are available, but in combination with depreciated protein force fields. In this work, a united-atom model of the lipid 1,2-dipalmitoyl-*sn*-glycero-3-phosphocholine has been built with standard parameters of the force field GROMOS96 53a6 that reproduces the experimental area per lipid of a lipid bilayer within 3% accuracy to a value of  $0.623 \pm 0.011 \text{ nm}^2$  without the assumption of a constant surface area or the inclusion of surface pressure. In addition, the lateral self-diffusion constant and deuterium order parameters of the acyl chains are in agreement with experimental data. Furthermore, models for 1,2-dimyristoyl-*sn*-glycero-3-phosphocholine (DMPC), 1-palmitoyl-2-oleoyl-*sn*-glycero-3-phosphocholine (POPC), and 1-palmitoyl-2-oleoyl-*sn*-glycero-3-phosphoglycerol (POPG) result in areas per lipid of  $0.625 \text{ nm}^2$  (DMPC),  $0.693 \text{ nm}^2$  (POPC), and  $0.700 \text{ nm}^2$  (POPG) from 40 ns MD simulations. Experimental lateral self-diffusion coefficients are reproduced satisfactorily by the simulation. The lipid models can form the basis for molecular dynamics simulations of membrane proteins with current and future versions of united-atom protein force fields.

### Introduction

Proteins associated with lipid membranes constitute approximately 30% of genomes<sup>2</sup> and are estimated to form more than half of all drug targets.<sup>3</sup> However, because of well-known experimental problems in membrane protein structure determination, the number of atomic-resolution structures of soluble proteins far exceeds the number of membrane protein structures. Therefore, membrane proteins have been a popular target for computational modeling<sup>4</sup> as well as model building based on limited experimental data.<sup>5</sup> Additionally, the slowly growing repository of high-resolution membrane protein structures<sup>6</sup> forms a resource for atomic-level studies of function and conformational change. As membrane protein simulations with explicit solvents require in excess of 30 000 atoms, molecular dynamics (MD) simulations based on classical mechanics are usually applied.<sup>7,8</sup> A key ingredient of MD simulations is the force field composed of a set of mathematical functions and parameters that describe all of

the bonded and nonbonded interactions between particles. Widely used biomolecular force fields are Amber,<sup>9</sup> CHARMM,<sup>10</sup> OPLS-AA,<sup>11</sup> and GROMOS,<sup>12</sup> the first three of which are all-atom force fields, whereas GROMOS is a united-atom force field that subsumes nonpolar hydrogen atoms into their adjacent carbon atom. While the accuracy of the force fields for protein modeling is comparable,<sup>13</sup> the united-atom approach poses a distinct advantage for membrane systems, reducing the number of particles by up to 60%; for example, a united-atom model of 1,2-dipalmitoyl-*sn*-glycero-3-phosphocholine (DPPC) is composed of 50 particles, while the corresponding all-atom model consists of 130 particles. Accurate force field parameters and lipid models are available for the all-atom CHARMM force field.<sup>14,15</sup> Additionally, lipid models for the all-atom General Amber Force Field (GAFF) have been developed recently<sup>16,17</sup> that required the incorporation of surface tension in order to achieve the experimental lipid surface area. For the CHARMM force field, a united-atom model of 1-palmitoyl-2-oleoyl-*sn*-glycero-3-phosphocholine (POPC) is available<sup>18</sup> that was

\* Author e-mail: a.kukol@herts.ac.uk.

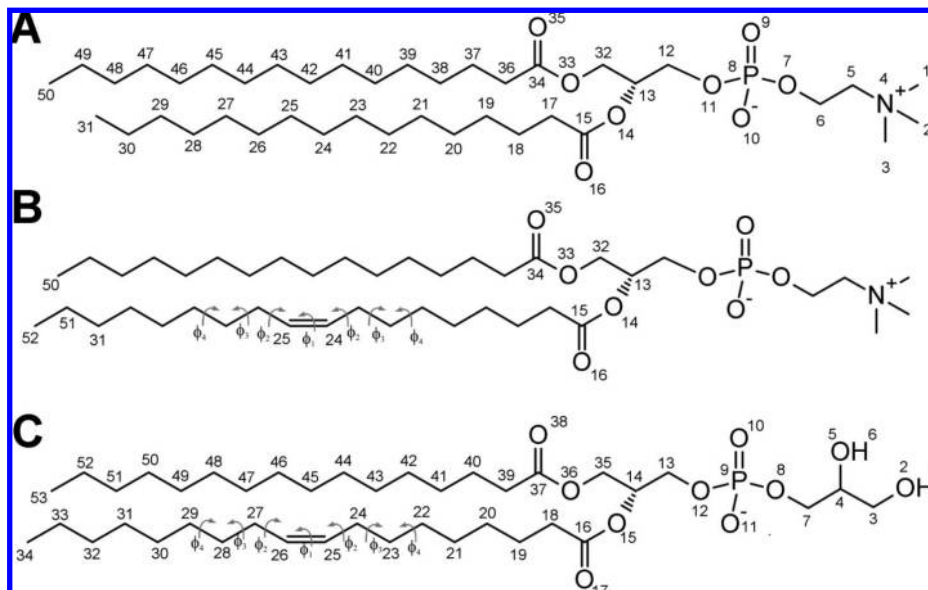


**Figure 1.** Definition of the atom numbers and torsion angles for the lipid models DPPC (A), POPC (B), and POPG (C).

used with constant area simulations in order to reproduce the experimental area per lipid ratio. Most united atom models of lipid molecules are based on the parameters developed by Berger et al.<sup>19</sup> within the united atom version of the OPLS force field.<sup>20</sup> Lipid models based on the Berger et al. parameters have been transferred to the united-atom GROMOS87 force field and used successfully for many lipid membrane MD simulations and membrane proteins. The united atom models for various lipids have successfully reproduced the most widely cited experimental data of area per lipid molecule within 2% accuracy as well as self-diffusion constants and order parameters for lipid bilayers without inclusion of surface tension or constant area simulations. Since GROMOS87,<sup>21</sup> the GROMOS force field has undergone significant revisions, with GROMOS96 in 1996<sup>22</sup> up to the latest versions 53a5 and 53a6 of the GROMOS96 force field.<sup>12</sup> The model of the DPPC lipid included in the latest 53a6 and previous versions of the force field distribution has unfortunately failed to reproduce the experimental parameters of DPPC membranes to satisfactory accuracy, as shown by various studies<sup>23,24</sup> as well as in this report. This has led to the paradoxical situation where many recent united-atom membrane protein simulations have used the GROMOS87 force field with lipid parameters based on Berger et al.<sup>25–28</sup> The problem with this approach is that MD simulations reproduce lipid bilayer attributes very well, while the membrane protein at the focus of interest may not be treated with comparable accuracy to other modern protein force fields. Some studies used a combination of the united-atom Berger et al. parameters and the all-atom OPLS force field, but the combination of different force fields is not straightforward and requires considerable care.<sup>29</sup> Ideally, lipid models should be developed with the same atom types, bonded and nonbonded parameters that are applied to the protein.

In order to support molecular dynamics simulations focused on membrane proteins, this work reports the development and evaluation of models of DPPC, 1,2-dimyristoyl-*sn*-glycero-3-phosphocholine (DMPC), POPC, and

1-palmitoyl-2-oleoyl-*sn*-glycero-3-phosphoglycerol (POPG) with GROMOS96 53a6 force field parameters that reproduce the experimental area/lipid ratio to a sufficient accuracy, in cases where experimental data for comparison is available. The lipid bilayer coordinates after 40 ns of MD simulations as well as the lipid models (topologies) are available as Supporting Information.

## Methods

**Initial Structures.** Initial coordinates of a 128-lipid DPPC bilayer hydrated with 3655 water molecules based on 2 ns equilibration,<sup>30</sup> a 128-lipid DMPC bilayer<sup>31</sup> with 3655 water molecules, and a POPC bilayer<sup>32</sup> with 2460 water molecules have been obtained from P. Tielman's Web site (<http://moose.bio.ucalgary.ca>). The initial coordinates of a 128-molecule POPG bilayer neutralized with 128 Na<sup>+</sup> counterions and hydrated with 3527 water molecules<sup>33</sup> have been obtained from M. Karttunen's Web site (<http://www.apmaths.uwo.ca/~mkarttu>). The racemic POPG bilayer was composed of equal numbers of L-POPG and D-POPG.

**Molecular Topologies.** For DPPC simulations, three different models (topologies) were investigated on the basis of the topology included in the GROMOS96 53a6 force field distribution. DPPC1 uses the original topology file without any alterations. DPPC2 has been modified with the partial charges of the lipid headgroup due to Chiu et al.,<sup>34</sup> with a subdivision into four charge groups as suggested by Chandrasekhar et al.<sup>24</sup> (model C in that publication). DPPC3 uses the partial charges model of DPPC2 with a different ester-carbonyl carbon atom type, "CH0" instead of "C" as suggested previously.<sup>24</sup> This resulted in a van der Waals radius for the carbonyl-ester of 0.664 nm for atom type "CH0", as opposed to 0.336 nm for atom type "C". The atom numbering scheme of all lipid models is shown in Figure 1.

The DMPC model was based on DPPC3, with two united-atom CH<sub>2</sub> groups less in each aliphatic carbon chain.

The POPC1 model adopted the same partial charges distribution for the lipid headgroup and torsion potentials as

**Table 1.** POPC Atom and Bond Parameters for the C=C Double Bond<sup>a</sup>

atom 1	atom 2	atom 3	atom 4	code	remark
24				CR1	
25				CR1	
24	25			gb_10	double bond
23	24	25		ga_27	
24	25	26		ga_27	
23	24	25	26	gi_1	improper dihedral

<sup>a</sup>For the definition of atom numbers, see Figure 1b. The meaning of the codes is given in the publication describing the GROMOS96 53a6 force field.<sup>12</sup>

**Table 2.** Atom Types and Charges for the POPG Head Group<sup>a</sup>

atom no.	code	charge
1	H	0.4170
2	OA	-0.5740
3	CH2	0.1570
4	CH1	0.1570
5	OA	-0.5740
6	H	0.4170
7	CH2	0.4000
8	OE	-0.8000
9	P	1.7000
10	OM	-0.8000
11	OM	-0.8000
12	OE	-0.7000
13	CH2	0.4000
14	CH1	0.3000
15	OE	-0.7000
16	CH0	0.7000
17	O	-0.7000

<sup>a</sup>For the definition of atom numbers, see Figure 1c. The meaning of the codes is given in the publication describing the GROMOS96 53a6 force field.<sup>12</sup>

DPPC3, while different bonded parameters were used in order to model the double bond, as shown in Table 1. The model POPC2 contains additional torsion potentials in the vicinity of the double bond (shown in Figure 1B), which have been developed previously by Bachar et al.<sup>35</sup> on the basis of ab initio calculations. The potentials included are

$$V(\varphi_2) = -5.865 + 7.470[1 + \cos(\varphi_2 - 180^\circ)] + 3.99[1 + \cos(2\varphi_2)] + 1.1[1 + \cos(3\varphi_2 - 180^\circ)]$$

$$V(\varphi_3) = 3.35[1 + \cos(\varphi_3)] - 1.66[1 + \cos(2\varphi_3 - 180^\circ)] + 7.333[1 + \cos(3\varphi_3)]$$

For computational efficiency, the torsion potential  $V(\phi_1)$  has been left unchanged as a standard Gromos96<sup>12</sup> improper torsion potential, and  $V(\phi_4)$  is described as Gromos96 dihedral type 34. It has been shown that the dihedral angle distributions for  $\phi_1$  and  $\phi_4$  with Bachar et al. potentials are similar to the situation where standard potentials are used.<sup>36</sup>

The POPG model provided by Karttunen et al.<sup>33</sup> (for the two stereoisomers D-POPG and L-POPG) has been translated into the GROMOS96 53a6 topology, while the partial charges for the glycerol headgroup have been retained. Atom types and charges are shown in Table 2. Bond and bond angle parameters are shown in Table 3, and torsion potentials for the lipid headgroup are shown in Table 4. The carbon chains of POPG1 have been modeled in the same way as

**Table 3.** Bond and Bond Angle Parameters for the POPG Head Group<sup>a</sup>

atom 1	atom 2	atom 3	code
1	2		gb_1
2	3		gb_13
3	4		gb_27
4	5		gb_13
5	6		gb_1
4	7		gb_27
7	8		gb_18
8	9		gb_28
9	10		gb_24
9	11		gb_24
9	12		gb_28
12	13		gb_18
14	15		gb_27
15	16		gb_10
16	17		gb_5
1	2	3	ga_12
2	3	4	ga_13
3	4	5	ga_13
4	5	6	ga_12
5	4	7	ga_13
3	4	7	ga_13
4	7	8	ga_13
4	7	8	ga_15
7	8	9	ga_26
8	9	10	ga_14
8	9	11	ga_14
8	9	12	ga_5
9	12	13	ga_26
10	9	11	ga_29
10	9	12	ga_14
11	9	12	ga_14
12	13	14	ga_15
13	14	15	ga_13
13	14	35	ga_13
14	15	16	ga_22
14	35	36	ga_15
15	14	35	ga_13
15	16	17	ga_31
15	16	18	ga_16
16	18	19	ga_15

<sup>a</sup>For the definition of atom numbers, see Figure 1c. The meaning of the codes is given in the publication describing the GROMOS96 53a6 force field.<sup>12</sup>

POPC1, while for POPG2, the Bachar et al.<sup>35</sup> torsion potentials have been included as described above for POPC2. A POPG3 model has been generated that is identical to POPG1, apart from the atom type "C" for the ester carbonyl atom, as used before in DPPC1 and DPPC2. The topologies are available as Supporting Information.

**ErbB2 Transmembrane Domain Simulation.** The starting coordinates of the ErbB2 transmembrane domain sequence GCPAEQRASPLTSIIASVVGILLVVVLGVVFGI-LIKRRQKIRK were obtained from the RCSB Protein Data Bank<sup>37</sup> (PDB ID: 2JWA). This structure was originally obtained by NMR spectroscopy from the peptide in 1,2-dihexanoyl-*sn*-glycero-3-phosphocholine/DMPC bicelles at 313 K.<sup>38</sup> For the MD simulation, the peptide was inserted into a pre-equilibrated DMPC lipid bilayer using a series of scaling and energy minimization steps, as described by Kandt et al.<sup>39</sup> Chloride ions were added at positions of most favorable electrostatic potential in order to neutralize the system. The resulting peptide/lipid/ions/water system contained 103 DMPC molecules, 12 chloride ions, and 5749 water molecules. MD simulations were carried out with the

**Table 4.** Torsion Potentials for the POPG Head Group<sup>a</sup>

atom 1	atom 2	atom 3	atom 4	code
1	2	3	4	gd_23
6	5	4	7	gd_23
5	4	7	8	gd_18
2	3	4	5	gd_18
2	3	4	7	gd_33
2	3	4	7	gd_17
3	4	5	6	gd_23
3	4	7	8	gd_33
3	4	7	8	gd_17
4	7	8	9	gd_29
7	8	9	12	gd_20
7	8	9	12	gd_27
8	9	12	13	gd_20
8	9	12	13	gd_27
9	12	13	14	gd_29
12	13	14	15	gd_34
12	13	14	35	gd_34
12	13	14	35	gd_17
13	14	35	36	gd_34
13	14	35	36	gd_17
13	14	15	16	gd_29
14	35	36	37	gd_29
14	15	16	18	gd_13
15	14	35	36	gd_18
15	16	18	19	gd_40

<sup>a</sup> For the definition of the atom numbers, see Figure 1c. The meaning of the codes is given in the publication describing the GROMOS96 53a6 force field.<sup>12</sup>

**Table 5.** Overview of Simulations Performed<sup>a</sup>

model	features
DPPC1	original model included in GROMOS96 53a6 force field
DPPC2	based on DPPC1, different partial charges of the headgroup atoms
<b>DPPC3</b>	based on DPPC2, larger carbonyl-ester atoms, atom type "CH0"
<b>DMPC</b>	same as DPPC3 with shorter acyl chains
POPC1	based on DPPC3, with unsaturated chain
<b>POPC2</b>	based on POPC1, changed torsion potentials next to double bond
POPG1	based on POPC1, with glycerol headgroup
<b>POPG2</b>	based on POPC2, with glycerol headgroup
POPG3	based on POPC1, smaller carbonyl-ester type "C" (data not shown)
ErbB2/DMPC	ErbB2 transmembrane peptide with GROMACS force field and Berger lipids
<b>ErbB2/DMPC</b>	ErbB2 transmembrane peptide and lipids with GROMOS96 53a6 force field

<sup>a</sup> Models in boldface are recommended and included in the Supporting Information.

GROMACS force field based on GROMOS87 and Berger et al.<sup>19</sup> lipid parameters and, in addition, with the GROMOS96 53a6 force field and the DMPC model developed in the present study. The lipid and water molecules were allowed to equilibrate around the peptide during a 10 ns MD simulation at 314 K with position restraints applied to the peptide atoms. The position restraint MD simulation was followed by unrestrained MD simulations over 20 ns. All simulations performed are summarized in Table 5.

**Simulation Parameters.** All simulations were performed with the GROMACS simulation package,<sup>40–42</sup> version 3.3.2. The NpT ensemble and periodic boundary conditions were used, while the temperature was kept constant with the Berendsen thermostat<sup>43</sup> at 325 K for all DPPC simulations,

at 314 K for DMPC, and at 298 K for POPC and POPG, with a coupling time constant of 0.1 ps. We chose the temperature such that it was at least 10 K above the gel to liquid-crystalline phase transition temperature. The phase transition temperature of POPC and POPG is below 273 K; therefore, the standard thermodynamic temperature of 298 K was chosen. Lipid and water molecules were coupled separately to the thermostat; in the case of POPG, water molecules and 128 sodium ions were jointly coupled to the thermostat. Semianisotropic Berendsen pressure coupling<sup>43</sup> was applied with separate coupling to the *z* direction (the bilayer normal) and the *xy* plane with a coupling time constant of 2.0 ps in order to maintain a constant pressure of 1.0 bar. For Lennard-Jones interactions, a cutoff at 1.4 nm was applied, while electrostatic interactions were treated with the particle mesh Ewald (PME) method<sup>44,45</sup> and a real-space cutoff of 0.9 nm. A larger than usual Lennard-Jones cutoff was used in order to increase the accuracy of the van der Waals interactions. Electrostatic interactions were treated with the PME method, which does not introduce artificial ordering like cutoff methods.<sup>46</sup> The real-space cutoff of 0.9 nm used with the PME method is merely a numerical device in order to separate the direct- and reciprocal-space sums. Long-range dispersion corrections for energy and pressure were applied. All systems were first subjected to 1000 steps of energy minimization, followed by a 40 ns MD simulation with a time step of 2 fs. The lipid molecule bonds were constrained with the LINCS algorithm,<sup>47</sup> while the water molecules were constrained with the SETTLE algorithm.<sup>48</sup> All simulations were carried out on a dual-processor dual-core AMD Opteron 2.66 GHz workstation (DNUK, Ashton-under-Lyne, United Kingdom).

**Data Analysis.** The area per lipid molecule was calculated from the lateral *x* and *y* dimensions of the simulation box divided by the number of lipid molecules in one leaflet of the bilayer. The reported average area per lipid was taken over the time from 20 to 40 ns.

Lateral diffusion coefficients for lipid molecules were calculated from the mean square displacement (MSD) of the center of mass  $\langle (r(t + \tau) - r(t))^2 \rangle$ , where  $\langle \rangle$  refers to the average taken over all starting times  $\tau$  and  $r(t)$  to the position of the center of mass at time *t*. The lateral diffusion coefficient is then given by the Einstein relation  $\text{MSD} = 4D_{\text{lat}}t$  in two dimensions for long times *t* and is averaged over 128 lipid molecules. In order to obtain the long-range diffusion coefficients, the MSD was fitted between 20 and 38 ns. Calculations have been performed with the *g\_msd* program of the GROMACS suite. Diffusion constants were not further corrected for random motions of the lipid monolayer, as it was found to be insignificant under periodic boundary conditions.

The deuterium order parameter  $S_{\text{CD}}$  for the carbon tails is calculated from the elements of the order parameter tensor  $S_{xx} = 1/2\langle (3 \cos^2 \alpha_i - 1)/2 \rangle$  and  $S_{yy}$  as  $S_{\text{CD}} = 2/3S_{xx} + 1/3S_{yy}$ . The angle  $\alpha_i$  is the angle between the molecular axis given by the carbon atoms  $C_{i-1}$  and  $C_{i+1}$  and the lipid bilayer normal; the average is taken over the time of 20–40 ns and for all lipid molecules. Calculations have been performed with the *g\_order* program of the GROMACS suite.



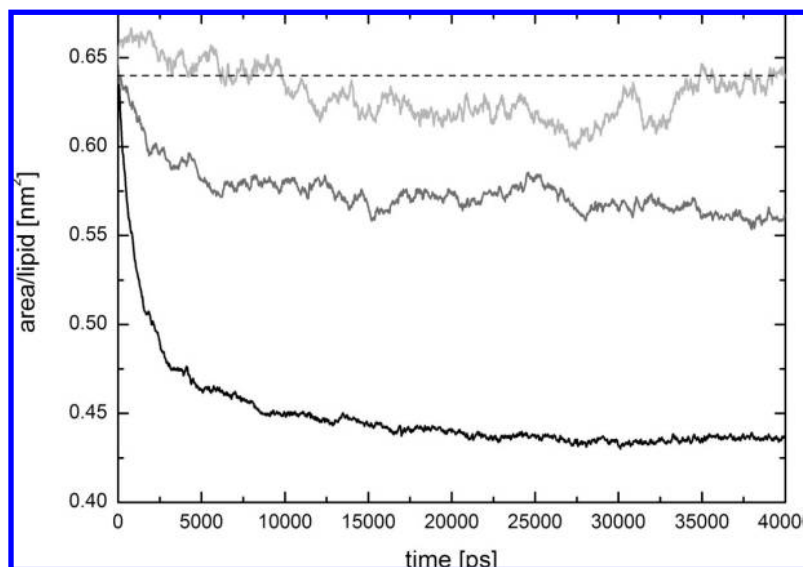


**Figure 2.** Area per lipid ratio dependent on MD simulation time for a 128-molecule lipid bilayer obtained with various lipid models: DPPC1 (black curve), DPPC2 (dark gray), and DPPC3 (light gray). The lipid models are explained in the text. The dashed line indicates the currently accepted experimental value for the area per lipid ratio.<sup>50</sup>

The radial distribution function of water hydrogens averaged between 20 and 40 ns around the ester carbonyl atoms of the *sn1* and *sn2* chains was calculated with the *g\_rdf* program of the GROMACS suite.

The angles between the P–N vector of the lipid headgroups and the *z* axis were calculated with a Perl script developed in-house.

## Results

**DPPC.** Lipid bilayers with three different DPPC models have been subjected to 40 ns MD simulation, and the time evolution of the area per lipid molecule has been calculated. The area per lipid molecule is the most widely used parameter for the characterization of lipid bilayers, as it is related to various other properties of the membrane like the lateral diffusion, membrane elasticity, or permeation. Figure 2 shows the area per lipid dependent on time for three different DPPC models. From the curves in Figure 2, the equilibration time of the simulation has been estimated qualitatively as less than 20 ns; thus, the period between 20 and 40 ns has been used to calculate average properties. For DPPC1, the original model included in the GROMOS force field distribution, the area per lipid reached an average of  $0.436 \pm 0.002 \text{ nm}^2$ . Model DPPC2, which has alternative headgroup charges according to Chiu et al.,<sup>34</sup> reached an average area per lipid of  $0.568 \pm 0.007 \text{ nm}^2$ , while the change of the ester carbonyl atom type from “C” to “CH0” in model DPPC3 led to an average area per lipid of  $0.623 \pm 0.011 \text{ nm}^2$ , which is within a range of 3% of the experimental value of around  $0.64 \text{ nm}^2$ .<sup>49,50</sup>

The deuterium order parameters  $|S_{CD}|$  dependent on the carbon atom number along the hydrocarbon tails show excellent agreement with experimental data<sup>51</sup> (Figure 3). There is some deviation from the experimental results for carbon-2 of the *sn1* chain, which corresponds to atom number 36 in Figure 1A.

The interactions between lipid and water molecules have been analyzed by calculating the radial distribution function of water hydrogens around the carbonyl-ester atoms for the *sn1* and *sn2* chains of DPPC (Figure 4). It is obvious from prominent peaks of the radial distribution function that water effectively solvates the carbonyl-oxygen atoms of both chains in the DPPC3 model (solid line). The more water-exposed carbonyl atom of the *sn2* chain achieves a stronger solvation, as indicated by the higher peak amplitude of the radial distribution function. In clear contrast, the DPPC1 model (dotted line) shows no significant solvation by water hydrogen atoms.

The molecular basis of these results can be seen in the snapshot of the simulation trajectory of a lipid bilayer constructed with DPPC1 (Figure 5A) and that constructed with DPPC3 (Figure 5B), both taken at 40 ns. The DPPC3 bilayer shows water penetrating into the lipid headgroup region, and the lipid acyl chains seem to be in a clearly disordered liquid-crystalline state, while acyl chains are highly ordered in the case of DPPC1 (Figure 5A). The same liquid-crystalline state is adopted by DPPC2 (not shown).

The angle between the lipid headgroup dipole moment as defined by the P–N vector and the *z* axis is  $90^\circ \pm 2$  for DPPC1,  $91^\circ \pm 3$  for DPPC2, and  $90^\circ \pm 2$  for DPPC3, averaged over all lipid molecules during the last 20 ns of the simulation. This is similar to the starting structure obtained from a previous simulation,<sup>30</sup> which yields an angle of  $89^\circ \pm 2$  between the P–N vector and the *z* axis averaged over 128 lipid molecules.

The lateral diffusion of lipid molecules is characterized by fast fluctuations in the limited space provided by surrounding lipids as well as by long-range diffusion throughout the lipid bilayer leaflet. The long-range diffusion coefficient for DPPC3 given in Table 6 shows good agreement with experimental data obtained from the literature.

**DPMPC, POPC, and POPG.** Lipid models (topologies) for DMPC, POPC, and POPG are not provided with the

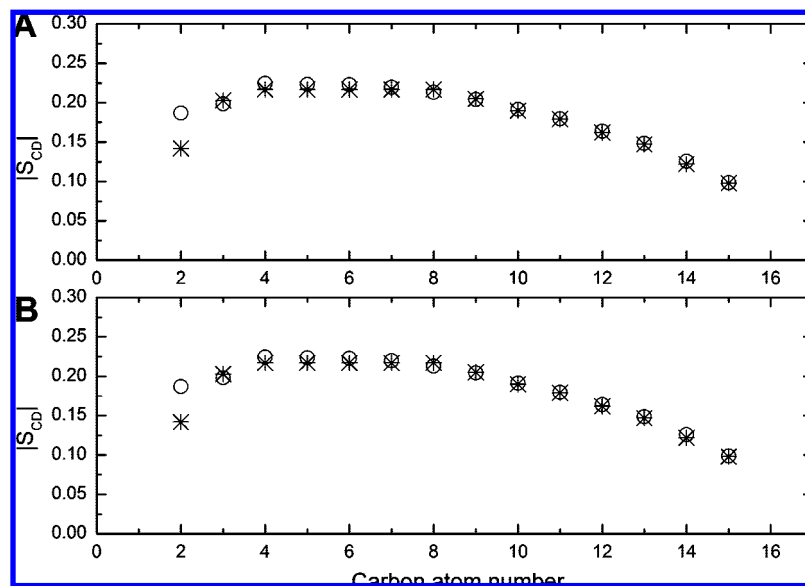


**Figure 3.** Comparison of the deuterium order parameters along the carbon atoms of the lipid acyl tails from simulation (○) and those from experimental results (\*). (A) The *sn1* chain. (B) The *sn2* chain. The experimental values are from the *sn2* chain in both parts.

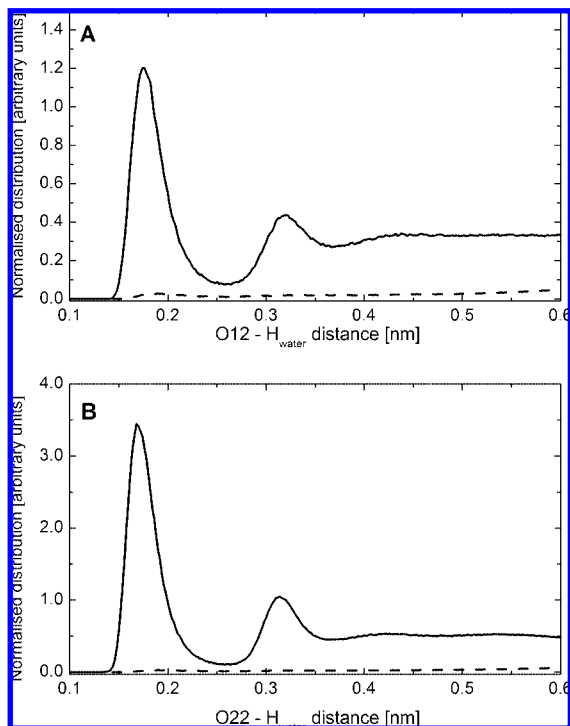


**Figure 4.** The radial distribution function of water hydrogens around the carbonyl-ester atoms for the *sn1* (A) and *sn2* (B) chains of DPPC. The radial distribution function has been normalized with respect to density and volume. The solid line represents the data obtained from simulation with the DPPC3 model, while the dotted line has been obtained with the DPPC1 model. The average between 20 and 40 ns has been taken.

GROMOS force field distribution. On the basis of the DPPC3 model, the DMPC model has been created by reducing the number of carbon atoms from 16 to 14 in each acyl chain and leaving all other parameters unchanged. The change of area per lipid ratio with simulation time shown in Figure 6 reveals that the bilayer is equilibrated almost immediately,

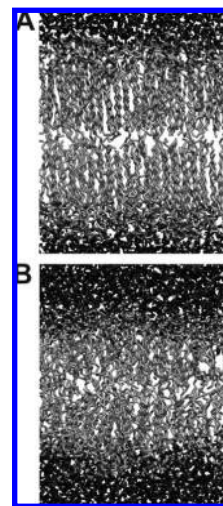


**Figure 5.** Snapshot of the MD simulation trajectory at 40 ns with the lipid models DPPC1 (A) and DPPC3 (B). The figure was created with VMD.<sup>1</sup>

because the DMPC bilayer based on Berger et al.<sup>19</sup> parameters has been used as the initial structure. The area per lipid averaged over the last 20 ns of the trajectory reaches a value of  $0.625 \pm 0.005 \text{ nm}^2$ , and the lipid lateral diffusion constant is  $5.7 \times 10^{-8} \pm 0.3 \text{ cm}^2 \text{ s}^{-1}$  (Table 6).

Two models of POPC have been evaluated. The POPC1 model is based on DPPC3, while different atom types, bond types, and torsion potentials (Table 1) have been used in order to model the double bond. In POPC2, the torsion potentials for bonds adjacent to the double bond ( $\phi_2$  and  $\phi_3$  in Figure 1B) have been replaced with potentials developed by Bachar et al.<sup>35</sup> The area per lipid ratio equilibrates for both models after 5 ns and reaches an average value of  $0.654 \pm 0.008 \text{ nm}^2$  for POPC1 and  $0.693 \pm 0.005 \text{ nm}^2$  for POPC2, which is closer to the experimental value of  $0.683 \text{ nm}^2$  (Table 6). The lateral diffusion constant of POPC1 is  $3.0 \times 10^{-8} \pm$

**Table 6.** Comparison of Area Per Lipid,  $A_{\text{sim}}$ , and Lateral Self Diffusion Coefficients  $D_{\text{sim}}$  Averaged from Trajectories between 20 and 40 ns for Various Lipid Models to Experimental Data ( $A_{\text{exp}}$ ,  $D_{\text{exp}}$ )

lipid	$A_{\text{sim}}$ [nm <sup>2</sup> ]	$A_{\text{exp}}$ [nm <sup>2</sup> ]	$D_{\text{sim}}$ [ $10^{-8}$ cm <sup>2</sup> s <sup>-1</sup> ]	$D_{\text{exp}}$ [ $10^{-8}$ cm <sup>2</sup> s <sup>-1</sup> ]
DPPC1	0.436 ± 0.002	0.64 <sup>a</sup>	3.0 ± 0.3	9.7
DPPC2	0.568 ± 0.007	0.64 <sup>a</sup>	8.2 ± 0.6	9.7
DPPC3	0.623 ± 0.011	0.64 <sup>a</sup>	6.8 ± 0.4	9.7 <sup>d</sup>
DMPC	0.625 ± 0.005	0.606 <sup>b</sup>	5.7 ± 0.3	14.3 <sup>e</sup>
POPC1	0.654 ± 0.008	0.683 <sup>c</sup>	3.0 ± 0.1	8.87
POPC2	0.693 ± 0.005	0.683 <sup>c</sup>	7.4 ± 0.3	8.87 <sup>e</sup>
POPG1	0.635 ± 0.008	N/A <sup>f</sup>	7.0 ± 0.2	3.0 <sup>g</sup>
POPG2	0.700 ± 0.007	N/A <sup>f</sup>	7.1 ± 0.5	3.0 <sup>g</sup>

<sup>a</sup> Reference 50. <sup>b</sup> Reference 57. <sup>c</sup> Reference 64. <sup>d</sup> Reference 65 (at 333 K). <sup>e</sup> Reference 52. <sup>f</sup> 0.64 nm<sup>2</sup> for PG prepared from egg Lecithin,<sup>59</sup> 0.66 nm<sup>2</sup> for a DPPC/DMPG (50:50) monolayer.<sup>66</sup> <sup>g</sup> Reference 67 (obtained from NBD-PG in a supported planar bilayer composed of 22% POPC and 76.5% POPG).

0.1 cm<sup>2</sup> s<sup>-1</sup> and is  $7.4 \times 10^{-8} \pm 0.3$  cm<sup>2</sup> s<sup>-1</sup> for POPC2, which is closer to the experimental value of  $8.9 \times 10^{-8}$  cm<sup>2</sup> s<sup>-1</sup>.<sup>52</sup>

The POPG1 model uses the same parameters for the acyl chains as those of POPC1, while the parameters of the headgroup are shown in Tables 2–4. The charges of the headgroup atoms are the same as those used by Zhao et al.<sup>33</sup> The POPG2 model includes the torsion potentials for bonds adjacent to the double bond analogous to POPC2. The area per lipid ratio after 20 ns reaches an average value of  $0.635 \pm 0.008$  nm<sup>2</sup> for POPG1 and  $0.700 \pm 0.007$  nm<sup>2</sup> for POPG2, while the lateral diffusion coefficient is  $7.0 \times 10^{-8} \pm 0.2$  cm<sup>2</sup> s<sup>-1</sup> for POPG1 and  $7.1 \times 10^{-8} \pm 0.5$  cm<sup>2</sup> s<sup>-1</sup> for POPG2.

In general, the area per lipid values of DPPC3, DMPC, and POPC2 averaged from the trajectories between 20 and 40 ns show excellent agreement with experimental results (Table 6). The lateral diffusion constants are of the right order of magnitude, when compared to experimental values (Table 6), although it should be noted that the experimental conditions were sometimes different from the simulation, for example, using fluorescently labeled POPG molecules in order to measure the diffusion constant.

Since the area per lipid for POPG simulations is different from those of other simulation studies (see Discussion), an analysis of the sodium ion distribution has been conducted. The distribution of sodium ions with respect to the bilayer normal ( $z$  axis) is shown in Figure 7A for the POPG2 bilayer. Sodium ions penetrate deeply into the lipid headgroup region; the peak values of the sodium atom density are reached at a position deeper into the lipid bilayer than the peak values of the phosphorus atom density.

Sodium atoms are found hexagonally coordinated with the involvement of one or two lipid molecules, while the free coordination sites are occupied by water molecules (Figure 7B). In the bulk water, sodium ions are coordinated hexagonally and pentagonally (Figure 7B). The ester-carbonyl oxygens of the lipid molecules participate in sodium coordination as well as the oxygen atoms of glycerol hydroxyl groups or oxygen atoms of the phosphate ester group (P–O–C). There is no example of the participation

of terminal oxygens of the phosphate groups in sodium coordination. Similar findings have been reported by Zhao et al.,<sup>33</sup> albeit with a much smaller area per lipid ratio.

**Transmembrane Peptide Simulation.** Since the ultimate aim was to use the lipid models for united-atom membrane protein simulations, the ErbB2 transmembrane domain has been subjected to 20 ns MD simulation using the established GROMOS87/Berger lipids force field combination as well as the GROMOS96 53a6 force field. Visual analysis of the trajectory showed that both simulations maintained the secondary structure and the integrity of the transmembrane helix dimer. Structural fluctuations occurred mainly in the unstructured regions outside the lipid bilayer. The root-mean-square deviation (rmsd) of the protein backbone with respect to the starting structure shown in Figure 8 increased over the first 1000 ps to a value in the region of 0.33 nm. Both force fields behaved initially identically until 7000 ps, where the rmsd values began to diverge. The backbone rmsd averaged between 10 and 20 ns was  $0.31 \text{ nm} \pm 0.02$  for the GROMOS96 53a6 force field and  $0.42 \text{ nm} \pm 0.02$  for the GROMOS87 force field. A similar divergence was observed for MD trajectories with different random initial atom velocities.

## Discussion

The development and evaluation of various lipid models with standard GROMOS96 53a6 force field parameters has been shown. For DPPC, the most studied lipid molecule, the important experimental area per lipid ratio has been reproduced with the DPPC3 model to a reasonable accuracy of 3% by simulations. The initial improvement of the area per lipid ratio seen in Figure 2 on going from model DPPC1 to DPPC2 is caused by the increased penetration of water into the lipid bilayer headgroup region due to the higher partial charges on the headgroup atoms in the DPPC2 model, as reported before.<sup>23</sup> The increased water penetration can be seen clearly from the comparison of the radial distribution functions of water around lipid carbonyl-ester (Figure 4) between DPPC1 and DPPC3 (the same for DPPC2, not shown). Additionally the dipole–dipole interaction between the lipid headgroups may affect the area per lipid, as discussed by Wohler and Edholm.<sup>55</sup> The in-plane component of the headgroup dipole contributes to attractive forces, while the components perpendicular to the membrane plane repel each other. The angle between the P–N vector and the  $z$  axis was found to be around 90° in all cases, which would contribute to attractive forces. The dipole moment of the headgroup is similar for DPPC1 and DPPC2, because the sum of the charges on the phosphate group (–1) and the choline group (+1) is the same for both charge schemes. It is due to the larger atomic charges of the DPPC2 headgroup that water penetrated into the lipid headgroup region and thus overcame parts of the attractive forces. Additionally, the use of the PME scheme for the treatment of electrostatics renders the system less vulnerable to electrostatic artifacts introduced by the cutoff scheme.<sup>55</sup>

The further increase of the area per lipid in the DPPC3 model is caused by the larger radius of the ester carbon of



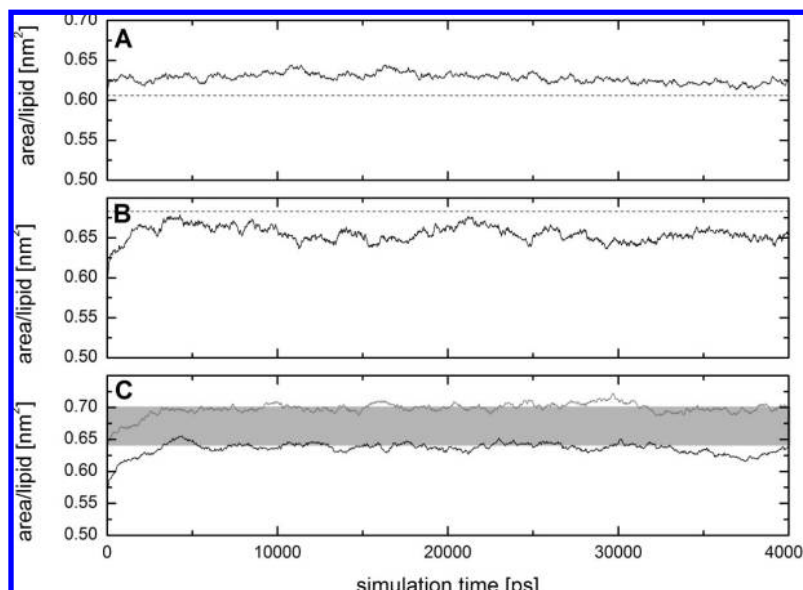


**Figure 6.** Area per lipid ratio dependent on MD simulation time for a 128-molecule lipid bilayer composed of (A) DMPC, (B) POPC2, and (C) POPG1 (dark curve) and POPG2 (gray curve). The dashed lines indicate the experimental value, and the gray shaded area indicates a probable range of experimental area per lipid ratios for POPG.

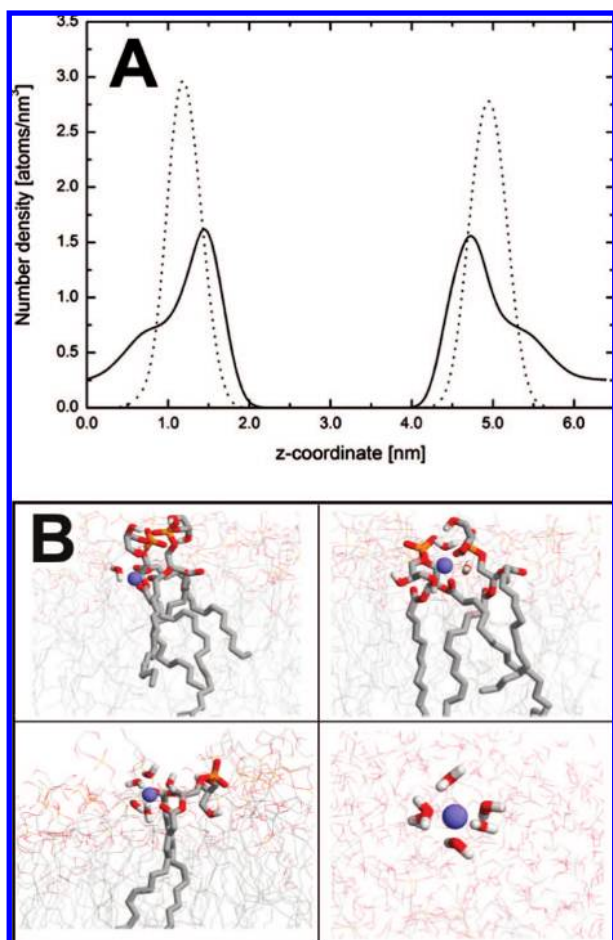


**Figure 7.** Characteristic features of the POPG bilayer. Panel A shows the atom number density of sodium (solid line) and phosphorus (dotted line) dependent on the *z* coordinate, the normal to the bilayer plane. Panel B shows snapshots from the MD trajectory taken at 38 ns of various modes of sodium interactions with lipid and water molecules. Panel B was created with Rasmol.<sup>53,54</sup>

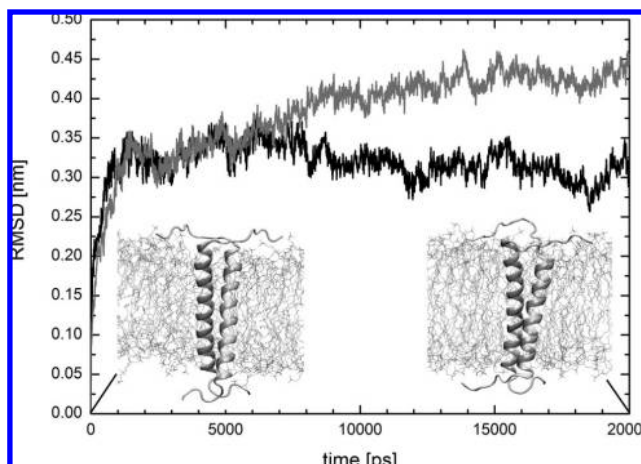


**Figure 8.** Root-mean-square deviation (rmsd) of the backbone atoms with respect to the experimental structure for the MD simulation of the ErbB2 transmembrane peptide dimer in a DMPC lipid membrane with the GROMOS96 53a6 force field (black curve) and the GROMACS force field (gray curve). The insets show the experimental structure (left) and a snapshot of the MD trajectory taken at 20 000 ps from the GROMOS96 simulation (right).

0.664 nm in the DPPC3 model compared to the 0.336 nm chosen in the DPPC1 and DPPC2 models. The molecular picture of Figure 5 reveals that additionally the disorder of the acyl chains is markedly increased for the DPPC3 model, as would be expected for a liquid-crystalline phase. The addition of further torsion potentials to the DPPC3 model did not yield any improvement in the area per lipid ratio, but a slight decrease to 0.61 nm<sup>2</sup>/lipid was seen (data not shown). Furthermore, the experimental deuterium order parameters and the diffusion coefficients are well reproduced by the DPPC3 model (Figure 3 and Table 6). It can be concluded that the DPPC3 model with an area per lipid of  $0.623 \pm 0.011$  nm<sup>2</sup> achieves high accuracy compared to experimental data. The results are in line with other studies



based on the Berger et al.<sup>19</sup> model, which achieve even higher accuracy, for example, 0.645 nm<sup>2</sup> in a study by Patra et al.<sup>46</sup> or 0.655 nm<sup>2</sup> in another recent study.<sup>56</sup> The advantage of the lipid model presented here is that it is fully compatible with the recent GROMOS96 53a6 force field. Therefore, we recommend the DPPC3 lipid model for united-atom membrane protein MD simulations.

The lipid bilayer based on the DMPC model showed an equally satisfactory reproduction of experimental parameters.

The increased area per lipid ratio of the POPC1 lipid bilayer is most likely caused by the increased lipid bilayer packing disorder introduced by the *cis* double bond in the lipid acyl chain. The inclusion of more realistic torsion potentials for the bonds adjacent to the double bond in POPC2 further increases the area per lipid to  $0.693 \pm 0.005$  nm<sup>2</sup>, which is within 1.5% of the experimental result of 0.683 nm<sup>2</sup>.<sup>57</sup> This is the best reproduction of the area per lipid ratio for POPC in the literature so far, to our knowledge. The all-atom lipid models using the CHARMM force field required constant area simulations or the application of surface pressure,<sup>58</sup> similar to a recent DOPC model using GAFF.<sup>17</sup> A recent simulation of 128 POPC<sup>33</sup> using the united-atom parameters of Berger et al.<sup>19</sup> achieved 0.658 nm<sup>2</sup>.

The area per lipid for the POPG1 model reaches 0.635 and 0.700 nm<sup>2</sup> for POPG2. On the basis of the improved agreement between simulation and experimental results of the area per lipid for POPC2 due to the inclusion of modified torsion potentials, POPG2, which includes the same torsion potentials as POPC2, is chosen as the preferred model. There are no experimental data of the area per lipid ratio for pure POPG lipid membranes in the liquid-crystalline state available, to our knowledge. Phosphatidyl-glycerol of various chain lengths and compositions prepared from egg lecithin yielded an area per lipid of 0.64 nm<sup>2</sup> using X-ray diffraction<sup>59</sup> (extracted from Figure 1 in that publication). A DPPC/DMPC (50:50) lipid monolayer gave a value of 0.66 nm<sup>2</sup> from neutron reflection data. These values most likely underestimate the area per lipid of a pure POPG lipid bilayer, since an unsaturated acyl chain is expected to increase the surface area of a lipid molecule, as can be seen from the comparison between DPPC and POPC. DMPG used in the monolayer study has completely saturated acyl chains, and PG lipids prepared from egg lecithin contain a large amount of saturated chains. A more recent X-ray study of the negatively charged phospholipid 1,2-dioleoyl-*sn*-glycero-3-phospho-L-serine in the fluid state obtained a surface area per lipid of 0.653 nm<sup>2</sup> in the fluid state and in the absence of osmotic pressure.<sup>60</sup> Until further experimental data become available, the POPG2 model with a lipid surface area of 0.700 nm<sup>2</sup> agrees more with the experimental data mentioned above than the POPG1 model.

It is interesting to note that most other MD simulation studies so far report much smaller area per lipid ratios for POPG bilayers. For example, a study by Zhao et al.<sup>33</sup> reports a value of 0.530 nm<sup>2</sup>, and Elmore<sup>61</sup> reports a value of 0.561 nm<sup>2</sup>. Another simulation study of a POPE/POPG (75:25) mixture<sup>62</sup> obtains an area per lipid ratio for POPG of 0.628 nm<sup>2</sup> from a decomposition of the area into POPG and POPE contributions using a Voronoi tessellation method. This result

is not directly comparable to a pure POPG system, since the POPG area is most likely influenced by the presence of POPE. Other simulations of lipids with negatively charged headgroups obtain a similar small area per lipid ratio; for example, for POPS, a value of 0.55 nm<sup>2</sup> has been found.<sup>63</sup> The smaller lipid surface area of charged lipids in comparison to neutral lipids is explained by the binding of counterions that not only compensate for the electrostatic repulsion of the negatively charged headgroups but lead to a further condensation of the bilayer area. Of note is the deviation of the area per lipid in our study (POPG1, 0.635 nm<sup>2</sup>) from the previous study by Zhao et al.<sup>33</sup> (0.530 nm<sup>2</sup>), which used a similar POPG model with the same partial charge distribution. In the same study, Zhao et al. obtained an average area per lipid of 0.658 nm<sup>2</sup> for POPC, which is identical with our result for POPC1, taking into account the error margin. In order to rationalize these differences, further simulations of POPG1 have been conducted, where the van der Waals radius of the ester-carbonyl atoms has been changed from 0.664 to 0.336 nm ("CH0" to "C" atom type). The "C" atom type has been used in the DPPC1 and DPPC2 models, which led to an unsatisfactory reproduction of the area per lipid. For POPG, this resulted in an average area per lipid of  $0.573 \pm 0.004$  nm<sup>2</sup>, which is similar to simulation results reported by other groups. However, in light of available experimental data, as discussed above, an area per lipid of 0.700 nm<sup>2</sup> seems more accurate. The likely reason for the larger area per lipid in our work is the van der Waals repulsion between sodium atoms in the lipid headgroup region and lipid atoms. There is the possibility that previous MD simulations of anionic lipid bilayers underestimated the surface area per lipid, because they did not model the space requirements of the lipid-bound counterions adequately. Future experimental studies of pure POPG and POPS lipid bilayers are required in order to provide a final answer.

The new DMPC/GROMOS96 53a6 lipid model has been compared to the Berger et al.<sup>19</sup>/GROMOS87 lipid model in membrane protein simulations. During a 20 ns simulation, the lipid/force field combination developed in this work showed better performance in maintaining the experimental structure, as revealed by the rmsd deviation. The experimental conditions for ErbB2 structure determination of DHPC/DMPC bicelles are similar but not identical to a pure DMPC bilayer. Therefore, deviation from the experimental structure as a measure of force field quality has to be considered with caution. Unfortunately, most membrane protein structures have been obtained at conditions far different from a liquid-crystalline lipid bilayer, for example, from crystals in X-ray crystallography or from detergent micelles in NMR spectroscopy.

In conclusion, united-atom lipid models for DPPC, DMPC, POPC, and POPG have been developed that accurately reproduce experimental data and should enable researchers to carry out united-atom membrane protein simulations with the latest 53a6 version of the GROMOS96 force field, thus reducing the computational costs as compared to all-atom force fields without sacrificing significantly the accuracy of the simulation.

**Acknowledgment.** This work was supported by the School of Life Sciences at the University of Hertfordshire, United Kingdom.

**Supporting Information Available:** The atomic coordinates of the bilayer systems and topology files of the lipid molecules are provided. This material is available free of charge via the Internet at <http://pubs.acs.org>.

## References

- (1) Humphrey, W.; Dalke, A.; Schulten, K. VMD: visual molecular dynamics. *J. Mol. Graphics* **1996**, *14* (1), 33–38; 27–28.
- (2) Wallin, E.; von Heijne, G. Genome-wide analysis of integral membrane proteins from eubacterial, archaean, and eukaryotic organisms. *Protein Sci.* **1998**, *7* (4), 1029–1038.
- (3) Terstappen, G. C.; Reggiani, A. In silico research in drug discovery. *Trends Pharmacol. Sci.* **2001**, *22* (1), 23–26.
- (4) Sperotto, M. M.; May, S.; Baumgaertner, A. Modelling of proteins in membranes. *Chem. Phys. Lipids* **2006**, *141* (1–2), 2–29.
- (5) Kukul, A. Site-specific IR spectroscopy and molecular modelling combined towards solving transmembrane protein structure. *Spectrosc. Int. J.* **2005**, *19* (1), 1–16.
- (6) White, S. H. Membrane proteins of known 3D structure. [http://blanco.biomol.uci.edu/Membrane\\_Proteins\\_xtal.html](http://blanco.biomol.uci.edu/Membrane_Proteins_xtal.html) (accessed Dec 15, 2008). University of California at Irvine.
- (7) Biggin, P. C.; Bond, P. J. Molecular dynamics simulations of membrane proteins. *Methods Mol. Biol.* **2008**, *443*, 147–60.
- (8) Lindahl, E. R. Molecular dynamics simulations. *Methods Mol. Biol.* **2008**, *443*, 3–23.
- (9) Cornell, W. D.; Cieplak, P.; Bayly, C. I.; Gould, I. R.; Merz, K. M.; Ferguson, D. M.; Spellmeyer, D. C.; Fox, T.; Caldwell, J. W.; Kollman, P. A. A 2nd Generation Force-Field for the Simulation of Proteins, Nucleic-Acids, and Organic-Molecules. *J. Am. Chem. Soc.* **1995**, *117* (19), 5179–5197.
- (10) MacKerell, A. D.; Bashford, D.; Bellott, M.; Dunbrack, R. L.; Evanseck, J. D.; Field, M. J.; Fischer, S.; Gao, J.; Guo, H.; Ha, S.; Joseph-McCarthy, D.; Kuchnir, L.; Kuczera, K.; Lau, F. T. K.; Mattos, C.; Michnick, S.; Ngo, T.; Nguyen, D. T.; Prodhom, B.; Reiher, W. E.; Roux, B.; Schlenkrich, M.; Smith, J. C.; Stote, R.; Straub, J.; Watanabe, M.; Wiorkiewicz-Kuczera, J.; Yin, D.; Karplus, M. All-atom empirical potential for molecular modeling and dynamics studies of proteins. *J. Phys. Chem. B* **1998**, *102* (18), 3586–3616.
- (11) Jorgensen, W. L.; Maxwell, D. S.; Tirado-Rives, J. Development and testing of the OPLS all-atom force field on conformational energetics and properties of organic liquids. *J. Am. Chem. Soc.* **1996**, *118* (45), 11225–11236.
- (12) Oostenbrink, C.; Villa, A.; Mark, A. E.; Van Gunsteren, W. F. A biomolecular force field based on the free enthalpy of hydration and solvation: the GROMOS force-field parameter sets 53A5 and 53A6. *J. Comput. Chem.* **2004**, *25* (13), 1656–1676.
- (13) Guvench, O.; MacKerell, A. D. Comparison of protein forcefields for molecular dynamics simulations. *Methods Mol. Biol.* **2008**, *443*, 63–88.
- (14) Feller, S. E.; MacKerell, A. D. An improved empirical potential energy function for molecular simulations of phospholipids. *J. Phys. Chem. B* **2000**, *104* (31), 7510–7515.
- (15) Feller, S. E.; Gawrisch, K.; MacKerell, A. D. Polyunsaturated fatty acids in lipid bilayers: Intrinsic and environmental contributions to their unique physical properties. *J. Am. Chem. Soc.* **2002**, *124* (2), 318–326.
- (16) Rosso, L.; Gould, I. R. Structure and dynamics of phospholipid bilayers using recently developed general all-atom force fields. *J. Comput. Chem.* **2008**, *29* (1), 24–37.
- (17) Siu, S. W. I.; Vacha, R.; Jungwirth, P.; Bockmann, R. A. Biomolecular simulations of membranes: Physical properties from different force fields. *J. Chem. Phys.* **2008**, *128* (12), 125103–12115.
- (18) Henin, J.; Shinoda, W.; Klein, M. L. United-atom acyl chains for CHARMM phospholipids. *J. Phys. Chem. B* **2008**, *112* (23), 7008–7015.
- (19) Berger, O.; Edholm, O.; Jahnig, F. Molecular dynamics simulations of a fluid bilayer of dipalmitoylphosphatidylcholine at full hydration, constant pressure, and constant temperature. *Biophys. J.* **1997**, *72* (5), 2002–2013.
- (20) Jorgensen, W. L.; Tiradorives, J. The Opls Potential Functions for Proteins - Energy Minimizations for Crystals of Cyclic-Peptides and Crambin. *J. Am. Chem. Soc.* **1988**, *110* (6), 1657–1666.
- (21) Van Gunsteren, W. F.; Berendsen, H. J. C. *Groningen Molecular Simulation (GROMOS) Library Manual*; BIOS-MOS B.V.: Groningen, The Netherlands, 1987.
- (22) Daura, X.; Mark, A. E.; Van Gunsteren, W. F. Parametrization of aliphatic CH<sub>n</sub> united atoms of GROMOS96 force field. *J. Comput. Chem.* **1997**, *19* (5), 535–547.
- (23) Chandrasekhar, I.; Bakowies, D.; Glattli, A.; Hunenberger, P.; Pereira, C.; Van Gunsteren, W. F. Molecular dynamics simulation of lipid bilayers with GROMOS96: Application of surface tension. *Mol. Simul.* **2005**, *31* (8), 543–548.
- (24) Chandrasekhar, I.; Kastenholz, M.; Lins, R. D.; Oostenbrink, C.; Schuler, L. D.; Tieleman, D. P.; van Gunsteren, W. F. A consistent potential energy parameter set for lipids: dipalmitoylphosphatidylcholine as a benchmark of the GROMOS96 45A3 force field. *Eur. Biophys. J.* **2003**, *32* (1), 67–77.
- (25) Beevers, A. J.; Kukul, A. Systematic molecular dynamics searching in a lipid bilayer: application to the glycophorin A and oncogenic ErbB-2 transmembrane domains. *J. Mol. Graphics Modell.* **2006**, *25* (2), 226–33.
- (26) Liu, X.; Xu, Y.; Li, H.; Wang, X.; Jiang, H.; Barrantes, F. J. Mechanics of channel gating of the nicotinic acetylcholine receptor. *PLoS Comput. Biol.* **2008**, *4* (1), e19.
- (27) Cuthbertson, J. M.; Bond, P. J.; Sansom, M. S. P. Transmembrane helix-helix interactions: Comparative simulations of the glycophorin A dimer. *Biochemistry* **2006**, *45* (48), 14298–14310.
- (28) Haider, S.; Khalid, S.; Tucker, S. J.; Ashcroft, F. M.; Sansom, M. S. P. Molecular dynamics simulations of inwardly rectifying (Kir) potassium channels: A comparative study. *Biochemistry* **2007**, *46* (12), 3643–3652.
- (29) Tieleman, D. P.; MacCallum, J. L.; Ash, W. L.; Kandt, C.; Xu, Z. T.; Monticelli, L. Membrane protein simulations with a united-atom lipid and all-atom protein model: lipid-protein interactions, side chain transfer free energies and model proteins. *J. Phys.: Condens. Matter* **2006**, *18* (28), S1221–S1234.
- (30) Tieleman, D. P.; Berendsen, H. J. C. Molecular dynamics simulations of a fully hydrated dipalmitoyl phosphatidylcholine bilayer with different macroscopic boundary condi-

- tions and parameters. *J. Chem. Phys.* **1996**, *105* (11), 4871–4880.
- (31) Tieleman, D. P.; Berendsen, H. J.; Sansom, M. S. An alamethicin channel in a lipid bilayer: molecular dynamics simulations. *Biophys. J.* **1999**, *76* (4), 1757–1769.
- (32) Tieleman, D. P.; Berendsen, H. J. A molecular dynamics study of the pores formed by Escherichia coli OmpF porin in a fully hydrated palmitoyl-oleoyl-phosphatidylcholine bilayer. *Biophys. J.* **1998**, *74* (6), 2786–801.
- (33) Zhao, W.; Rog, T.; Gurtovenko, A. A.; Vattulainen, I.; Karttunen, M. Atomic-scale structure and electrostatics of anionic palmitoyl-oleoyl-phosphatidylglycerol lipid bilayers with Na<sup>+</sup> counterions. *Biophys. J.* **2007**, *92* (4), 1114–1124.
- (34) Chiu, S.-W.; Clark, M.; Subramaniam, B. S.; Scott, H. L.; Jacobson, E. Incorporation of surface tension into molecular dynamics simulation of an interface: a fluid phase lipid bilayer membrane. *Biophys. J.* **1995**, *69* (10), 1230–1245.
- (35) Bachar, M.; Brunelle, P.; Tieleman, D. P.; Rauk, A. Molecular dynamics simulation of a polyunsaturated lipid bilayer susceptible to lipid peroxidation. *J. Phys. Chem. B* **2004**, *108* (22), 7170–7179.
- (36) Martinez-Seara, H.; Rog, T.; Karttunen, M.; Reigada, R.; Vattulainen, I. Influence of cis double-bond parametrization on lipid membrane properties: How seemingly insignificant details in force-field change even qualitative trends. *J. Chem. Phys.* **2008**, *129*10.
- (37) Berman, H. M.; Westbrook, J.; Feng, Z.; Gilliland, G.; Bhat, T. N.; Weissig, H.; Shindyalov, I. N.; Bourne, P. E. The Protein Data Bank. *Nucleic Acids Res.* **2000**, *28* (1), 235–42.
- (38) Bocharov, E. V.; Mineev, K. S.; Volynsky, P. E.; Ermolyuk, Y. S.; Tkach, E. N.; Sobol, A. G.; Chupin, V. V.; Kirpichnikov, M. P.; Efremov, R. G.; Arseniev, A. S. Spatial structure of the dimeric transmembrane domain of the growth factor receptor ErbB2 presumably corresponding to the receptor active state. *J. Biol. Chem.* **2008**, *283* (11), 6950–6.
- (39) Kandt, C.; Ash, W. L.; Tieleman, D. P. Setting up and running molecular dynamics simulations of membrane proteins. *Methods* **2007**, *41*, 475–488.
- (40) Berendsen, H. J. C.; van der Spoel, D.; van Drunen, R. GROMACS: A message passing parallel molecular dynamics implementation. *Comput. Phys. Commun.* **1995**, *91*, 43–56.
- (41) Lindahl, E.; Hess, B.; van der Spoel, D. Gromacs 3.0: A package for molecular dynamics simulation and trajectory analysis. *J. Mol. Model.* **2001**, *7*, 306–317.
- (42) Van Der Spoel, D.; Lindahl, E.; Hess, B.; Groenhof, G.; Mark, A. E.; Berendsen, H. J. GROMACS: fast, flexible, and free. *J. Comput. Chem.* **2005**, *26* (16), 1701–18.
- (43) Berendsen, H. J. C.; Postma, J. P. M.; Vangunsteren, W. F.; Dinola, A.; Haak, J. R. Molecular-Dynamics with Coupling to an External Bath. *J. Chem. Phys.* **1984**, *81* (8), 3684–3690.
- (44) Darden, T.; York, D.; Pedersen, L. Particle Mesh Ewald - an N-Log(N) Method for Ewald Sums in Large Systems. *J. Chem. Phys.* **1993**, *98* (12), 10089–10092.
- (45) Essmann, U.; Perera, L.; Berkowitz, M. L.; Darden, T.; Lee, H.; Pedersen, L. G. A Smooth Particle Mesh Ewald Method. *J. Chem. Phys.* **1995**, *103* (19), 8577–8593.
- (46) Patra, M.; Karttunen, M.; Hyvonen, M. T.; Falck, E.; Lindqvist, P.; Vattulainen, I. Molecular dynamics simulations of lipid bilayers: major artifacts due to truncating electrostatic interactions. *Biophys. J.* **2003**, *84* (6), 3636–3645.
- (47) Hess, B.; Bekker, H.; Berendsen, H. J. C.; Fraaije, J. G. E. M. LINCS: A linear constraint solver for molecular simulations. *J. Comput. Chem.* **1997**, *18* (12), 1463–1472.
- (48) Miyamoto, S.; Kollman, P. A. Settle - An Analytical Version of the Shake and Rattle Algorithm for Rigid Water Models. *J. Comput. Chem.* **1992**, *13* (8), 952–962.
- (49) Nagle, J. F.; Tristram-Nagle, S. Lipid bilayer structure. *Curr. Opin. Struct. Biol.* **2000**, *10* (4), 474–480.
- (50) Kucerka, N.; Tristram-Nagle, S.; Nagle, J. F. Closer look at structure of fully hydrated fluid phase DPPC bilayers. *Bio-phys. J.* **2006**, *90* (11), L83–L85.
- (51) Douliez, J. P.; Leonard, A.; Dufourc, E. J. Restatement of Order Parameters in Biomembranes - Calculation of C-C Bond Order Parameters from C-D Quadrupolar Splittings. *Biophys. J.* **1995**, *68* (5), 1727–1739.
- (52) Filippov, A.; Oradd, G.; Lindblom, G. Influence of cholesterol and water content on phospholipid lateral diffusion in bilayers. *Langmuir* **2003**, *19* (16), 6397–6400.
- (53) Bernstein, H. J. Recent changes to RasMol, recombining the variants. *Trends Biochem. Sci.* **2000**, *25* (9), 453–5.
- (54) Sayle, R. A.; Milner-White, E. J. RASMOL: Biomolecular graphics for all. *Trends Biochem. Sci.* **1995**, *20* (9), 374.
- (55) Wohrlert, J.; Edholm, O. The range and shielding of dipole-dipole interactions in phospholipid bilayers. *Biophys. J.* **2004**, *87* (10), 2433–2445.
- (56) Patra, M.; Salonen, E.; Terama, E.; Vattulainen, I.; Faller, R.; Lee, B. W.; Holopainen, J.; Karttunen, M. Under the influence of alcohol: the effect of ethanol and methanol on lipid bilayers. *Biophys. J.* **2006**, *90* (4), 1121–35.
- (57) Kucerka, N.; Liu, Y. F.; Chu, N. J.; Petrache, H. I.; Tristram-Nagle, S. T.; Nagle, J. F. Structure of fully hydrated fluid phase DMPC and DLPC lipid bilayers using X-ray scattering from oriented multilamellar arrays and from unilamellar vesicles. *Biophys. J.* **2005**, *88* (4), 2626–2637.
- (58) Feller, S. E.; Pastor, R. W. Constant surface tension simulations of lipid bilayers: The sensitivity of surface areas and compressibilities. *J. Chem. Phys.* **1999**, *111* (3), 1281–1287.
- (59) Cowley, A. C.; Fuller, N. L.; Rand, R. P.; Parsegian, V. A. Measurement of Repulsive Forces between Charged Phospholipid Bilayers. *Biochemistry* **1978**, *17* (15), 3163–3168.
- (60) Petrache, H. I.; Tristram-Nagle, S.; Gawrisch, K.; Harries, D.; Parsegian, V. A.; Nagle, J. F. Structure and fluctuations of charged phosphatidylserine bilayers in the absence of salt. *Biophys. J.* **2004**, *86* (3), 1574–1586.
- (61) Elmore, D. E. Molecular dynamics simulation of a phosphatidylglycerol membrane. *FEBS Lett.* **2006**, *580* (1), 144–148.
- (62) Murzyn, K.; Rog, T.; Pasenkiewicz-Gierula, M. Phosphatidylethanolamine-phosphatidylglycerol bilayer as a model of the inner bacterial membrane. *Biophys. J.* **2005**, *88* (2), 1091–1103.
- (63) Mukhopadhyay, P.; Monticelli, L.; Tieleman, D. P. Molecular dynamics simulation of a palmitoyl-oleoyl phosphatidylserine bilayer with Na<sup>+</sup> counterions and NaCl. *Biophys. J.* **2004**, *86*, 1601–1609.
- (64) Kucerka, N.; Tristram-Nagle, S.; Nagle, J. F. Structure of fully hydrated fluid phase lipid bilayers with monounsaturated chains. *J. Membr. Biol.* **2005**, *208* (3), 193–202.
- (65) Konig, S.; Pfeiffer, W.; Bayerl, T.; Richter, D.; Sackmann, E. Molecular-Dynamics of Lipid Bilayers Studied by Incoher-

- ent Quasi-Elastic Neutron-Scattering. *J. Phys. II*. **1992**, 2 (8), 1589–1615.
- (66) Maierhofer, A. P.; Bucknall, D. G.; Bayerl, T. M. Modulation of cytochrome C coupling to anionic lipid monolayers by a change of the phase state: a combined neutron and infrared reflection study. *Biophys. J.* **2000**, 79 (3), 1428–1437.
- (67) Gilmanshin, R.; Creutz, C. E.; Tamm, L. K. Annexin-Iv Reduces the Rate of Lateral Lipid Diffusion and Changes the Fluid-Phase Structure of the Lipid Bilayer When It Binds to Negatively Charged Membranes in the Presence of Calcium. *Biochemistry* **1994**, 33 (27), 8225–8232.

CT8003468